Controlling FCCI with Pd in Metallic Fuel

Michael T. Benson, James A. King, Jason M. Harp, Robert D. Mariani

Idaho National Laboratory, P.O. Box 1625, MS 6188, Idaho Falls, ID 83415

Michael T. Benson, phone: (208) 533-8870, FAX: (208) 533-7863, email: michael.benson@inl.gov

Abstract. A major factor limiting the lifetime of U-Zr based fuel is fuel-cladding chemical interactions (FCCI). As the fuel is burned, fission product lanthanides (Ln) interact with the Fe-based cladding, causing thinning of the cladding wall and eventual breach of the cladding. In order to extend the lifetime of the fuel in reactor, FCCI must be controlled. Palladium has been shown to be a promising metallic fuel additive to control FCCI due to the stable Pd-Ln intermetallics formed. The current investigation is focused on the characterization of U-Zr-Pd fuel, with and without added lanthanides. Characterization includes as-cast fuel as well as annealed fuel, and comparison to recent post-irradiation examination results from U-10Zr fuel.
Key words: metallic fuel, FCCI, palladium-lanthanide precipitates

1. Introduction

Fuel-cladding chemical interaction (FCCI) occurs when the nuclear fuel or fission products react with the cladding material. A major cause of FCCI in U-Zr and U-Pu-Zr fuels during irradiation is fission product lanthanides (Ln), which tend to migrate to the fuel periphery, coming in contact with the cladding. The result of this interaction is degradation of the cladding, and will eventually lead to rupture of the fuel assembly.[1][2] Several methods are being investigated to decrease or prevent FCCI, such as barrier foils, coatings, and additive materials.[3][4][5] After considering ways to bind lanthanides as stable intermetallics, a set of criteria were developed that identified Pd as a promising additive, especially since it is already a fission product. Recent work using Pd as an additive has shown promising results.[5][7][8] Diffusion couples between Ln and iron (where Ln=Nd, Ce, Pr) show no interaction when Pd is present at 700°C, although in the absence of Pd, all three lanthanides interact strongly with Fe at 700°C.

Palladium is being investigated as an additive to control FCCI in metallic fuels specifically due to lanthanides. The lanthanides can burn-in as fission products, or can be present in the fresh fuel produced with recycled uranium. A small amount of lanthanides are expected to remain with uranium after pyroprocessing, thus being incorporated into a fresh fuel.[9] In this case, as soon as the fuel contacts the cladding due to swelling, at roughly 1-2% burnup, there are already lanthanides available to initiate FCCI. This is opposed to the much slower burn-in of fission product lanthanides in a fuel fabricated with clean uranium. Controlling FCCI in this system is even more important due to the potentially reduced lifetime of the fuel.[10]

The current study continues investigating Pd as a fuel additive. The as-cast and annealed microstructures are discussed for U-12Zr-4Pd and U-12Zr-4Pd-5Ln, and compared to post-irradiation examination (PIE) data from a U-10Zr fuel pin. Understanding how the alloys behave with palladium incorporated at reactor temperature is an important part of understanding how the alloys will behave as a fuel. The amount of lanthanides used in these alloys, 6.72 at%, corresponds to the amount of lanthanides produced at roughly 18% burn-up.[5] This is certainly much higher than expected in a fresh fuel produced with recycled uranium, but a high burn-up

fuel will reach this loading during irradiation. The composition and ratio of lanthanides are based on elemental analysis of irradiated U-10Zr EBR-II fuel pins,[5] with the four most prevalent lanthanides included in the mix. The ratio obtained from EBR-II fuel is 53Nd-25Ce-16Pr-6La, in wt %. In the case of recycled fuel, the starting concentrations of lanthanides will have a different elemental ratio. The separation factors for each lanthanide during the electro-refining operations, the starting lanthanide concentrations, and the specific conditions used during electrorefining will determine the ratio of lanthanides in the recycled fuel. Considering previous diffusion couple work,[7][8] varying the concentration of lanthanides present should not decrease the efficacy of Pd in binding the lanthanides.

2. Experimental Methods

Two alloys were cast, U-12Zr-4Pd wt% (67.6U-25.2Zr-7.2Pd at%) and U-12Zr-4Pd-5Ln (61.9U-24.5Zr-7.0Pd-6.6Ln at%), where Ln = 53Nd-25Ce-16Pr-6La wt% (52.3Nd-25.4Ce-16.2Pr-6.1La at%). All materials, except uranium, were obtained from Alfa Aesar and used as received. The lanthanides were obtained as rods, packaged in mylar under argon. Uranium was cleaned by submersion in nitric acid, followed by a water wash, then an ethanol wash.

All casting operations were carried out in an argon atmosphere glovebox with high purity argon as a cover gas in the arc melter. After each addition step, the resulting button was flipped and re-melted 3 times to ensure homogeneity. To prepare U-12Zr-4Pd, the appropriate amount of Pd, Zr, and U were arc melted together in two steps. The addition order was varied, as discussed below. To prepare 53Nd-25Ce-16Pr-6La, the appropriate amount of each lanthanide was arc melted together in one step. To prepare U-12Zr-4Pd-5Ln, the appropriate amount of the Ln alloy was added to U-12Zr-4Pd. The buttons were cast into 5mm diameter pins.

For the annealed samples, sections from each alloy were sealed in quartz under vacuum. The quartz tube was placed in a furnace at 650°C for 500 hours. After the heat treatment, the samples were quenched in water. The samples were cut to expose a fresh surface for analysis. Scanning electron microscopy (SEM) was performed on a 2 mm section of the pin mounted in a 31.8 mm diameter phenolic metallographic (met) mount filled with epoxy. Samples were polished by grinding the surfaces flat with SiC grinding paper followed by polishing with polycrystalline diamond suspensions, starting with 9µm, then 3 µm, and finally 1 µm. The polished sample was analyzed with a sputtered coating of approximately 15nm carbon to control charging of the met mount.

The post-irradiation sample is U-10Zr, from the MFF-3 assembly run in the Fast Flux Test facility (FFTF).[11] Details of this test and specific fuel pin have been previously reported.[2][12][13] This assembly had a peak inner cladding temperature of 643ºC and operated to 13.8 at.% burnup. The slice used for SEM analysis was taken at x/L=0.98 (fuel pin length=91.4cm) from fuel pin serial number 193045. The local burnup for the sample was 5.7 at.% and the time average temperature of the inner cladding for the sample was 615°C.[2]

The instrument used for sample analysis was a JSM-7600f SEM manufactured by the Japan Electron Optics Laboratory (JEOL). The JSM-7600f is a hot field emission SEM equipped with an Oxford Instruments X-Max 20 silicon drift energy dispersive X-ray spectrometer (EDS) and a Nordlys II F+ electron back scattered diffraction camera. The X-ray spectrometers are controlled by Oxford INCA software (v. 4.15, part of the Oxford Microanalysis Suite Issue 18d + SP 4), which also provides image acquisition capabilities.

The SEM was operated at an accelerating voltage of 20kV and a nominal beam current of approximately 50nA (which can vary somewhat with column conditions) for these analyses.

Prior to analysis, X-ray detector response was verified using a copper target. All of the X-ray spectra were accumulated for 100 live seconds. Spectra were collected over the energy range 0 – 20keV, which covers characteristic X-ray energies from all analytes.

Spectra were quantified using so-called "standardless" analysis, which uses a stored library of reference spectra to quantify unknown spectra rather than physical standards. This method is generally accurate to the 0.1 to 0.5 w/w% range, depending on sample and microscope (observation) conditions. Quantitative results for the alloys were normalized to only the alloy elements present.

3. Results and Discussion

The as-cast structure for U-12Zr-4Pd is shown in Figure 1, with accompanying EDS data listed in Table 1, respectively. The as-cast structure for U-12Zr-4Pd appears significantly different than previously reported,[5] due to the addition order during arc melting. In this alloy, Zr and Pd were combined prior to adding U. The Zr-Pd pre-alloy has an at% of 75Zr-25Pd, which should primarily be Zr_2Pd, based on the phase diagram.[14] EDS analysis indicates this intermetallic was carried over into the uranium alloy, and is the predominant Zr-Pd structure. Some of the Zr was pulled into the U-rich regions, allowing the formation of ZrPd as well. This alloy was used for the annealed studies discussed below. In the previous study,[5] U and Zr were combined first, followed by Pd addition. The Zr_2Pd and ZrPd precipitates are along the grain boundaries, with roughly double the amount of Zr remaining in the U-rich regions. Figure 2 shows the microstructure for U-12Zr-4Pd prepared in this manner, with EDS data listed in Table 2.

Results for the third possible permutation of elemental additions for alloying U-12Zr-4Pd, by first melting U and Pd, followed by Zr addition, is shown in Figure 3, with EDS data listed in Table 3. When first melting U and Pd, the pre-alloy is 95.5U-4.5Pd wt %, being predominantly α-U plus UPd_3. Some of the high melting UPd_3 (1640ºC) may remain in U-12Zr-4Pd, given the relatively high concentration of U in the precipitates (Table 3, dark 1-6), compared to the U concentration in the precipitates shown in Figure 1 (Table 1, dark 1-4). The microstructure is similar to that shown in Figure 1, although there is directionality to the precipitates. There is no obvious reason for this in the compositional analysis.

Further analysis of the U-12Zr-4Pd alloys shown in Figures 1-3 is underway. X-ray diffractometry (XRD) and differential scanning calorimetry(DSC) are in progress to determine if there are significant differences in the alloy properties.

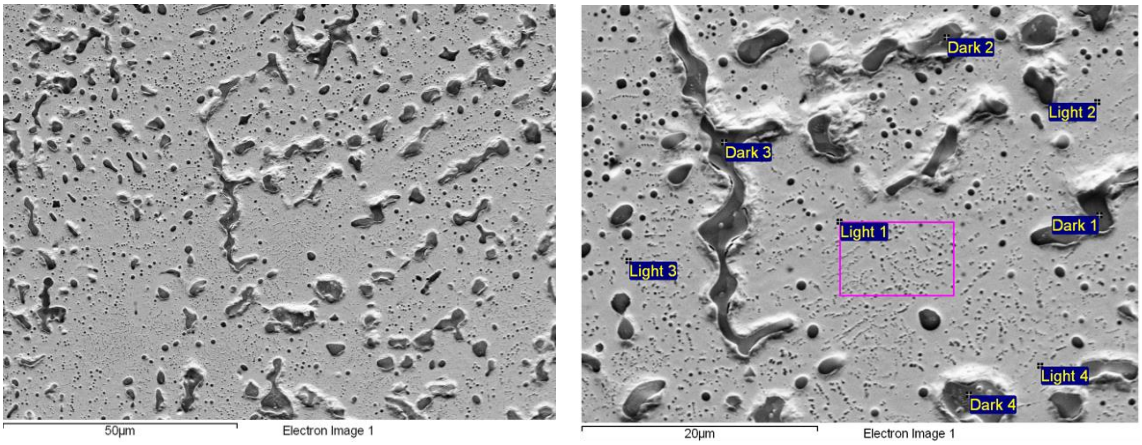

Figure 1. SEM low angle secondary electron image of as-cast U-12Zr-4Pd alloy (melt order: Zr+Pd followed by U). EDS results listed in Table 1. A large area scan shows the composition to be 83.7U-11.6Zr-4.7Pd (wt%).

TABLE 1. EDS RESULTS FOR POINTS SHOWN IN FIGURE 1. VALUES SHOWN IN WEIGHT % (ATOMIC %).

Spectrum	Zr	Pd	U
dark 1	43.0 (47.9)	52.9 (50.4)	4.1 (1.7)
dark 2	57.3 (63.3)	35.7 (33.7)	7.0 (3.0)
dark 3	55.0 (60.8)	38.6 (36.5)	6.4 (2.7)
dark 4	51.1 (61.5)	28.0 (28.9)	20.9 (9.6)
light 1	8.5 (19.0)	2.6 (4.9)	88.9 (76.1)
light 2	6.0 (14.0)	1.4 (2.8)	92.6 (83.2)
light 3	6.0 (14.1)	0.86 (1.7)	93.2 (84.2)
light 4	5.5 (13.1)	0.89 (1.8)	93.6 (85.1)

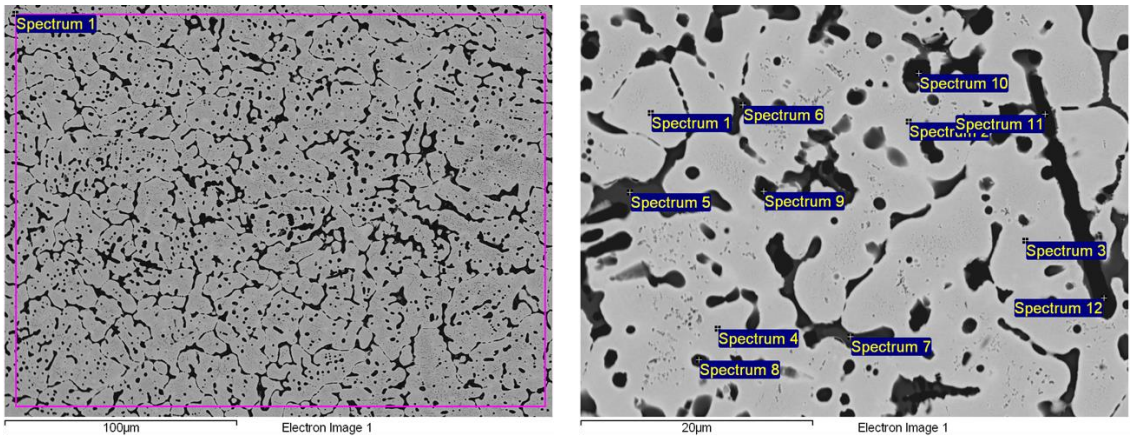

Figure 2. SEM backscatter image of as-cast U-12Zr-4Pd alloy (melt order: U+Zr followed by Pd). EDS results listed in Table 2. A large area scan shows the composition to be 82.61U-12.78Zr-4.61Pd (wt%).

TABLE 2. EDS RESULTS FOR POINTS SHOWN IN FIGURE 2. VALUES SHOWN IN WEIGHT % (ATOMIC %).

Spectrum	Zr	Pd	U
1	7.6 (17.5)	1.1 (2.1)	91.3 (80.4)
2	8.3 (18.9)	1.1 (2.1)	90.6 (79.0)
3	9.2 (20.7)	1.1 (2.2)	89.7 (77.1)
4	9.5 (21.2)	1.3 (2.5)	89.2 (76.3)
5	45.3 (50.1)	51.1 (48.4)	3.6 (1.5)
6	52.1 (60.3)	33.6 (33.3)	14.4 (6.4)
7	41.0 (48.1)	45.7 (46.0)	13.3 (6.0)
8	40.4 (48.8)	41.0 (42.5)	18.7 (8.7)
9	82.5 (89.3)	6.7 (6.3)	10.8 (4.5)
10	86.2 (91.6)	5.6 (5.1)	8.3 (3.4)
11	76.7 (84.0)	11.9 (11.2)	11.4 (4.8)
12	89.3 (93.4)	4.6 (4.1)	6.1 (2.5)

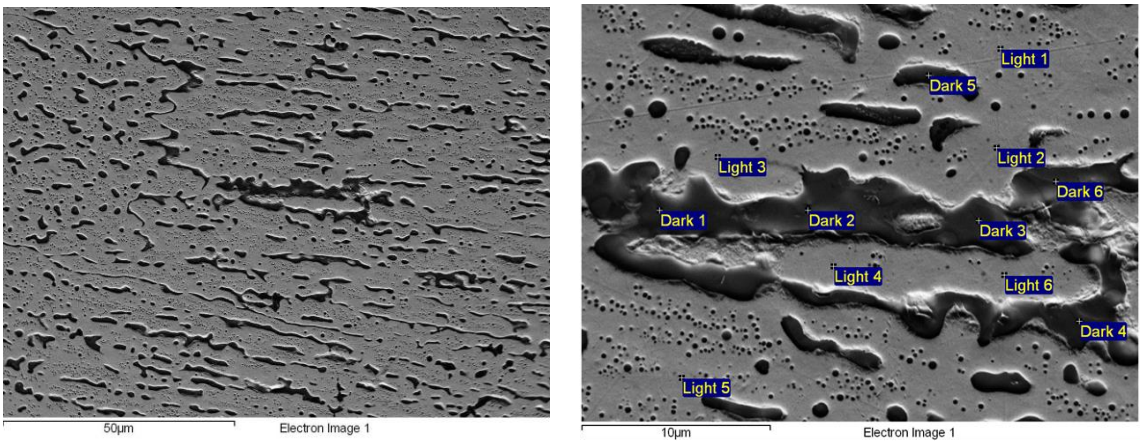

Figure 3. SEM low angle secondary electron image of as-cast U-12Zr-4Pd alloy (melt order: U+Pd followed by Zr). EDS results listed in Table 3. A large area scan shows the composition to be 83.7U-11.8Zr-4.5Pd (wt%).

TABLE 3. EDS RESULTS FOR POINTS SHOWN IN FIGURE 3. VALUES SHOWN IN WEIGHT % (ATOMIC %).

Spectrum	Zr	Pd	U
dark 1	51.1 (58.9)	35.5 (35.2)	13.4 (5.9)
dark 2	48.0 (59.2)	27.6 (29.2)	24.4 (11.5)
dark 3	53.5 (62.4)	30.4 (30.4)	16.1 (7.2)
dark 4	53.3 (60.1)	36.9 (35.7)	9.8 (4.2)
dark 5	39.9 (54.6)	21.5 (25.2)	38.6 (20.2)
dark 6	45.4 (53.1)	40.4 (40.5)	14.2 (6.4)
light 1	4.1 (10.0)	0.33 (0.7)	95.6 (89.3)
light 2	4.7 (11.3)	1.0 (2.1)	94.3 (86.7)
light 3	5.6 (13.2)	0.66 (1.3)	93.8 (85.4)
light 4	5.6 (13.3)	0.74 (1.5)	93.6 (85.2)
light 5	6.7 (15.5)	1.3 (2.5)	92.1 (82.0)
light 6	5.9 (14.0)	0.52 (1.1)	93.6 (84.9)

The as-cast structure for U-12Zr-4Pd-5Ln is shown in Figure 4, with EDS data listed in Table 4. This alloy was prepared in 3 steps, U-Zr was melting together first, followed by Pd addition, then Ln addition. The precipitates along the grain boundary are visible in the images

shown in Figure 3. This is very similar to the microstructure reported for U-15Zr-3.86Pd-4.3Ln, prepared with the same addition order.[5] The Ln-Pd inclusions are roughly 50Pd-50Ln, indicating the stable 1:1 intermetallic is being formed. There is more Zr found in the uranium matrix than in U-12Zr-4Pd, and a large number of black precipitates, comprised almost entirely of Zr, with very little Zr in the Ln-Pd precipitates. There is a small excess of Pd present compared to the lanthanides, 7.0Pd vs 6.6Ln at%, with a small amount found in the uranium matrix, and the rest in the black Zr precipitates.

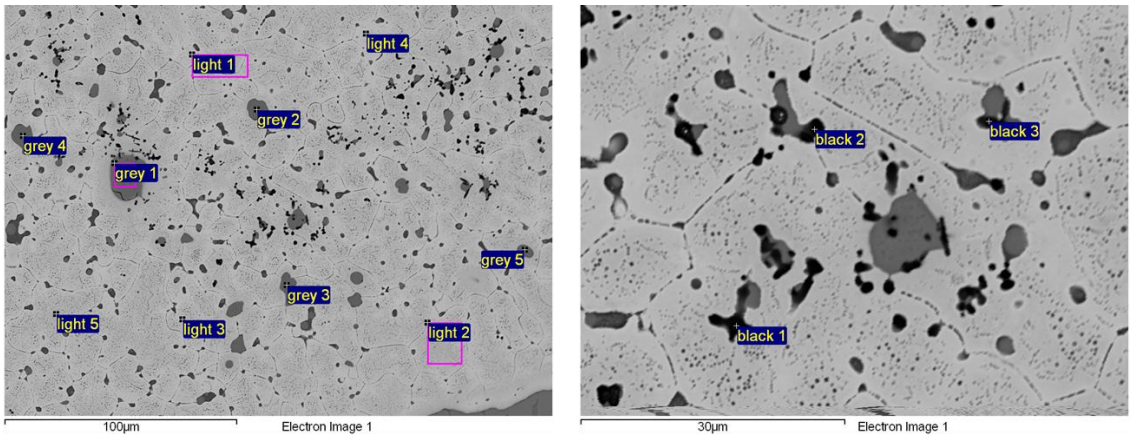

Figure 4. SEM backscatter images of as-cast U-12Zr-4Pd-5Ln. EDS results for both images listed in Table 4. A large area scan shows 79.2U-11.7Zr-4.3Pd-4.8Ln (wt%).

TABLE 4. EDS RESULTS FOR POINTS SHOWN IN FIGURE 4. VALUES SHOWN IN WEIGHT % (ATOMIC %).

Spectrum	Zr	Pd	U	Nd	Ce	Pr	La
grey 1	0.8 (1.1)	42.7 (50.1)	1.3 (0.7)	32.2 (27.8)	10.6 (9.4)	3.5 (3.0)	8.8 (7.8)
grey 2	4.6 (6.1)	42.3 (48.7)	2.0 (1.0)	25.6 (21.8)	15.2 (13.3)	2.3 (2.0)	8.1 (7.1)
grey 3	3.7 (5.0)	43.0 (49.6)	1.9 (1.0)	25.8 (22.0)	15.5 (13.5)	1.9 (1.7)	8.3 (7.3)
grey 4	6.9 (9.3)	41.1 (47.1)	3.0 (1.5)	24.2 (20.4)	15.1 (13.2)	1.3 (1.7)	7.8 (6.8)
grey 5	1.6 (2.1)	43.4 (50.7)	2.7 (1.4)	28.0 (24.2)	13.5 (12.0)	2.3 (2.1)	8.5 (7.6)
light 1	9.5 (21.1)	2.3 (4.3)	88.2 (74.6)	---	---	---	---
light 2	11.5 (24.6)	2.3 (4.3)	86.0 (70.8)	---	0.20 (0.3)	---	---
light 3	8.2 (18.6)	1.3 (2.5)	90.5 (78.8)	---	---	---	0.12 (0.2)
light 4	6.8 (15.8)	1.2 (2.4)	91.6 (81.3)	---	0.20 (0.3)	---	0.16 (0.2)
light 5	11.9 (25.5)	2.3 (4.2)	85.6 (70.1)	---	0.21 (0.3)	---	---
black 1	87.5 (93.9)	1.7 (1.5)	10.5 (4.3)	0.1 (0.1)	0.1 (0.1)	---	0.1 (0.1)
black 2	78.5 (88.4)	4.4 (4.2)	17.1 (7.4)	---	---	---	---
black 3	67.8 (80.1)	7.6 (7.7)	21.2 (9.6)	1.6 (1.2)	1.3 (1.0)	---	0.5 (0.4)

The annealed structure for U-12Zr-4Pd is shown in Figure 5, with EDS data listed in Table 5. The U-12Zr-4Pd alloy shown in Figure 1 was annealed, prepared by melting Zr and Pd, and then adding U. Based on the binary phase diagrams, the expected phases are present, i.e. α-U, δ-UZr_2, and $PdZr_2$. The light EDS points correspond to α-U, and the black points correspond to Zr precipitates. Nearly all of the Pd is incorporated in the globular $PdZr_2$ precipitates (grey EDS points). This removed Pd from the matrix, and also depletes Zr. The actual composition of the annealed alloy is 67.2U-24.3Zr-8.4Pd in at% (83.7U-11.6Zr-4.7Pd in wt%). Assuming all of the Pd is in the precipitates, 16.8Zr-8.4Pd at% is consumed in the precipitates, leaving roughly one third of the Zr in the matrix. A portion of the remaining Zr deposited as black precipitates,

further depleting Zr from the matrix. The low concentration of available Zr is evident by the small amount of δ-UZr_2 present (light grey EDS points), and the large amount of α-U, which dominates the microstructure.

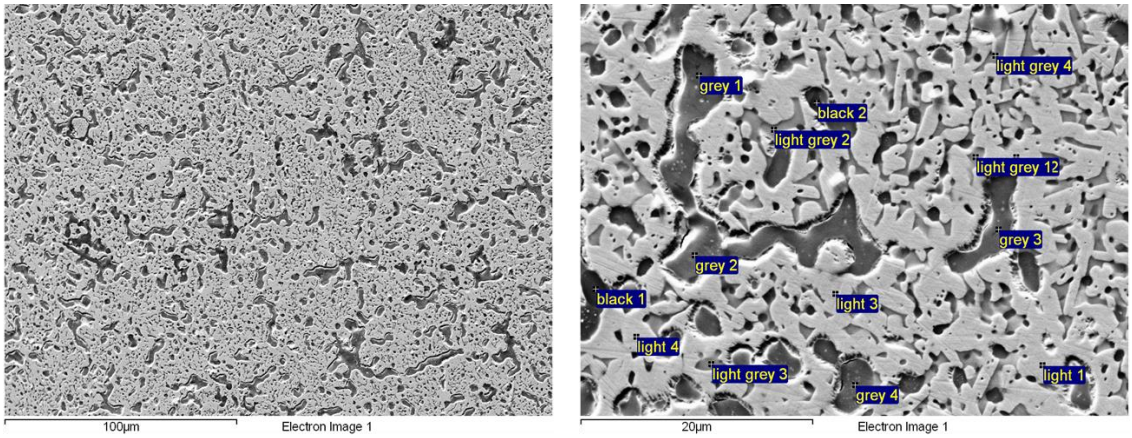

Figure 5. SEM low angle secondary electron image of annealed U-12Zr-4Pd alloy. EDS results listed in Table 5.

TABLE 5. EDS RESULTS FOR POINTS SHOWN IN FIGURE 5. VALUES SHOWN IN WEIGHT % (ATOMIC %).

Spectrum	Zr	Pd	U
grey 1	61.2 (65.6)	36.3 (33.3)	2.6 (1.1)
grey 2	58.9 (64.6)	34.8 (32.7)	6.4 (2.7)
grey 3	58.5 (64.7)	33.9 (32.1)	7.6 (3.2)
grey 4	55.7 (63.3)	32.3 (31.5)	12.0 (5.2)
black 1	92.6 (96.7)	0.7 (0.6)	6.7 (2.7)
black 2	72.6 (85.1)	4.6 (4.6)	22.8 (10.2)
light 1	0.5 (1.2)	0.8 (1.8)	98.7 (97.0)
light 2	0.5 (1.3)	0.8 (1.8)	98.7 (96.9)
light 3	0.4 (1.1)	0.7 (1.6)	98.8 (97.3)
light 4	0.4 (1.1)	0.7 (1.5)	98.9 (97.4)
light grey 1	33.3 (56.0)	1.2 (1.7)	65.5 (42.3)
light grey 2	28.0 (45.8)	11.7 (16.4)	60.3 (37.8)
light grey 3	34.8 (57.6)	1.3 (1.9)	63.9 (40.5)
light grey 4	31.6 (53.6)	2.6 (3.7)	65.8 (42.7)

The annealed microstructure for U-12Zr-4Pd-5Ln is shown in Figure 6, with EDS data listed in Table 6. The annealed structure with lanthanides included is significantly different from that shown in Figure 5. The large grey precipitates (EDS points grey 1-4) are the 1:1 Pd-lanthanide intermetallics. There is no uniformity in size for these precipitates, which ranged in size from single microns to several hundred microns. The white regions (EDS points light 1-4) are α-U, the light grey areas (EDS points light grey 1-4) are δ-UZr_2, and the black precipitates are Zr (EDS points black 1,2). An important observation in the annealed microstructure is the preference Pd has for the lanthanides. $PdZr_2$ is a stable intermetallic, as shown in the annealed microstructure for U-12Zr-4Pd, Figure 5, but nearly all of the Pd is in the Pd-Ln precipitates. The small amount of Pd outside the precipitates is likely due to the excess of Pd present in the alloy. The measured composition is 79.2U-11.7Zr-4.3Pd-4.8Ln in wt%, and 62.2U-24.0Zr-7.6Pd-6.3Ln in at%.

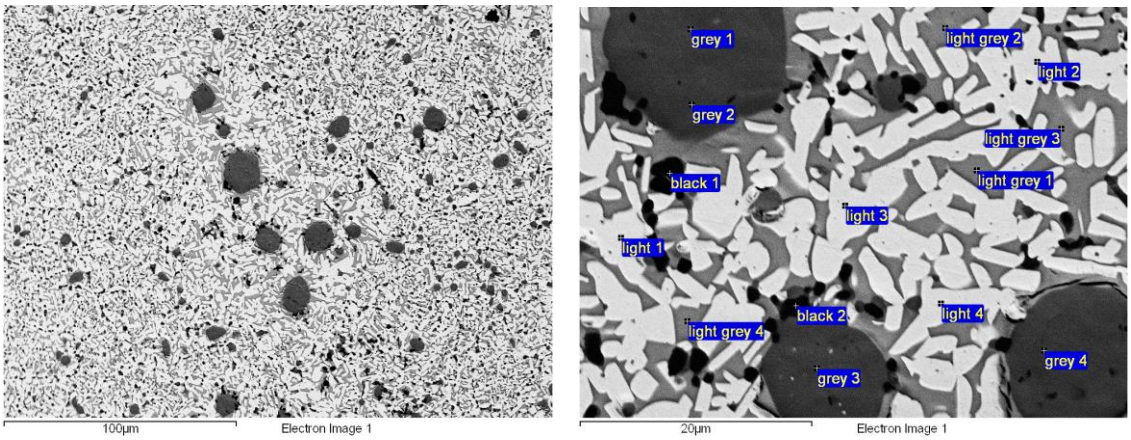

Figure 6. SEM backscatter images of annealed U-12Zr-4Pd-5Ln. EDS results listed in Table 6.

TABLE 6. EDS RESULTS FOR POINTS SHOWN IN FIGURE 6. VALUES SHOWN IN WEIGHT % (ATOMIC %).

Spectrum	Zr	Pd	U	Nd	Ce	Pr	La
grey 1	0.57 (0.8)	44.6 (51.7)	1.1 (0.6)	11.6 (9.9)	30.5 (26.9)	8.5 (7.4)	3.1 (2.8)
grey 2	0.50 (0.7)	44.9 (52.0)	0.9 (0.5)	10.9 (9.3)	31.6 (27.8)	8.4 (7.4)	2.8 (2.5)
grey 3	0.22 (0.3)	44.5 (51.6)	1.0 (0.5)	14.1 (12.1)	27.4 (24.2)	9.2 (8.0)	3.7 (3.3)
grey 4	0.25 (0.3)	44.8 (52.0)	0.82 (0.4)	13.3 (11.4)	27.6 (24.3)	9.0 (7.9)	4.2 (3.7)
light 1	0.31 (0.8)	0.73 (1.6)	98.9 (97.4)	---	---	0.10 (0.2)	---
light 2	0.31 (0.8)	0.71 (1.6)	98.5 (96.8)	0.23 (0.4)	---	0.26 (0.4)	---
light 3	0.31 (0.8)	0.70 (1.5)	98.6 (97.1)	0.18 (0.3)	---	0.17 (0.3)	---
light 4	0.38 (1.0)	0.71 (1.6)	98.9 (97.5)	---	---	---	---
black 1	89.0 (94.9)	0.94 (0.9)	9.6 (3.9)	0.20 (0.1)	0.27 (0.2)	---	---
black 2	84.3 (88.4)	6.7 (6.1)	2.0 (0.8)	2.1 (1.4)	3.6 (2.5)	0.97 (0.7)	0.35 (0.2)
light grey 1	36.8 (59.7)	1.3 (1.8)	61.7 (38.3)	0.12 (0.1)	---	0.12 (0.1)	---
light grey 2	38.8 (61.7)	1.3 (1.8)	59.5 (36.2)	0.18 (0.2)	---	0.12 (0.1)	---
light grey 3	39.3 (62.2)	1.3 (1.8)	59.2 (35.8)	0.18 (0.2)	---	---	---
light grey 4	39.7 (62.5)	1.3 (1.8)	58.8 (35.5)	0.24 (0.2)	---	---	---

The postirradiation microstructure from the MFF3 pin #193045 x/L=0.98 is shown in Figure 7 at high magnification. The majority of the striped microstructure is a mixture of α-U and δ-UZr_2. This region of the fuel is approximately 30 to 35 wt.% Zr by EDS analysis. The enhanced concentration of Zr in this area is due to the well-known phenomenon of Zr redistribution in irradiated U-Zr fuels. The key feature of Figure 7 is the dark grey precipitate highlighted by the red circle. This precipitate was characterized by EDS to be 27% Pd, 6% Y, 10% La, 15% Ce, and 41% Nd, in wt. %. The presence of this precipitate in this sample with fission product generated Pd is encouraging for the feasibility of this FCCI mitigation strategy.

The Pd present in this fuel is naturally produced, thus there is not enough Pd to bind the lanthanides in the 1:1 LnPd intermetallic. The measured amount of Pd, 27 wt%, will produce primarily Ln_7Pd_3, with a small amount of LnPd.[15] The Nd_7Pd_3 intermetallic has a melting point of 690°C, which is still higher than the peak fuel surface temperature of approximately 650°C. Data for the other Ln_7Pd_3 intermetallics are not available. Based on the similarities in the portions of the phase diagrams that are complete, the melting points for the other Ln_7Pd_3 intermetallics are expected to be similar to Nd_7Pd_3. The 1:1 LnPd intermetallic is nonetheless preferred, with a melting point of 950°C or higher, again based on available data.

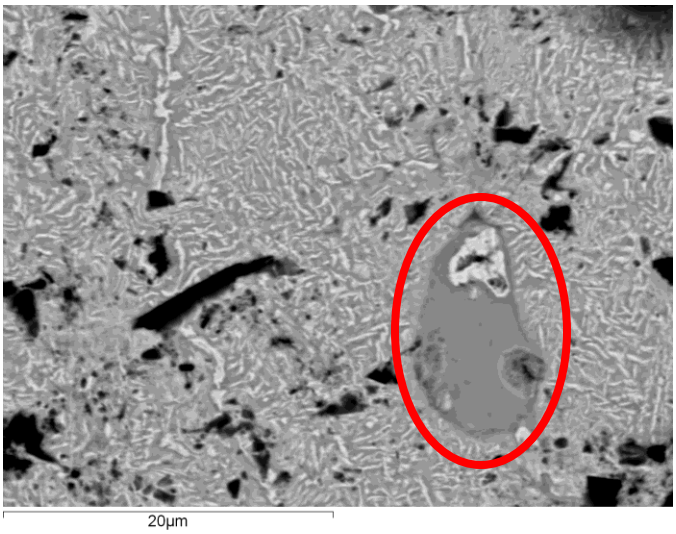

Figure 7. SEM backscatter image of FFTF fuel, post-irradiation.

4. Conclusions

U-12Zr-4Pd was fabricated with three different permutations for melting according to which two of the three elements are first melted. These three processes yielded significantly different microstructures.

The as-cast U-12Zr-4Pd-5Ln is very similar to the previously reported structure.[5] The annealed structure has LnPd precipitates, with the matrix comprised of δ-UZr_2 and α-U. This microstructure shows great promise for using Pd to control FCCI. The annealed structure for U-12Zr-4Pd, Figure 5, shows the affinity between Pd and Zr, after annealing U-12Zr-4Pd, the Zr is depleted from the matrix, and is found primarily in $PdZr_2$ precipitates. Due to this, there is very little δ-UZr_2, with the matrix mostly comprised of α-U. However, in the presence of lanthanides, Figure 6, there is essentially no Pd-Zr interaction. The Pd is shown to bind preferentially with the lanthanides over the zirconium. In actual fuel irradiations, this occurs for native Pd fission concentrations. The PIE image shown in Figure 7 shows definitively that Pd will bind the lanthanides, also indicating the promise Pd has in controlling the lanthanides and preventing FCCI.

Further experiments are in progress to determine if the microstructural differences due to fabrication order will impact the fuel performance or the ability of Pd to bind to the lanthanide fission products. Additional experiments include XRD and DSC, as well as annealing studies. In addition, PIE of Pd-doped fuel, whose alloy compositions have been described,[16] is presently underway.

Acknowledgments

The authors gratefully acknowledge the Department of Nuclear Energy, Office of Nuclear Energy, Science, and Technology, under DOE-NE Idaho Operations Office Contract DE-AC07-05ID14517.

References

[1] Keiser, D. D. "Fuel-Cladding Interaction Layers in Irradiated U-Zr and U-Pu-Zr Fuel Elements", Tech. Rep., Argonne National Laboratory-West (2006).

[2] Carmack, W. J., et al., "Metallography and fuel cladding chemical interaction in fast flux test facility irradiated metallic U-10Zr MFF-3 and MFF-5 fuel pins" J. Nucl. Mater. 473 (2016) 167-177.

[3] Lee, K. S., et al., "Effect of Zr Thin Film on Zr Foil as a FCCI Barrier Between Lanthanide (La-Ce) and Clad Material" Metals Mater. Intnl. 21 (2015) 498-503.

[4] Lo, W. Y.; Yang, Y. "Vanadium diffusion coating on HT-9 cladding for mitigating the fuel cladding chemical interactions" J. Nucl. Mater. 451 (2014) 137-142.

[5] Mariani, R. D., et al., "Lanthanides in metallic nuclear fuels: Their behavior and methods for their control" J. Nucl. Mater. 419 (2011) 263-271.

[6] D.D. Keiser, The development of fuel cladding interaction zones in irradiated U–Zr and U–Pu–Zr fuel elements with stainless steel cladding, in: A. Aasen, P. Olsson (Eds.), Nuclear Reactors, Nuclear Fusion and Fusion Engineering, Nova Science Publishers, New York (2009) 163–194.

[7] Egeland, G. W., et al., "Reduction of FCCI effects in lanthanide-iron diffusion couples by doping with palladium" J. Nucl. Mater. 440 (2013) 178-192.

[8] Egeland, G. W., et al., "Reducing fuel-cladding chemical interaction: The effect of palladium on the reactivity of neodymium on iron in diffusion couples" J. Nucl. Mater. 432 (2013) 539-544.

[9] Herrmann, S. D.; Li, S. X. "Separation and recovery of uranium metal from spent light water reactor fuel via electrolytic reduction and electorefining" Nucl. Tech. 171 (2010) 247-265.

[10] R. D. Mariani, et al., ATALANTE 2012, Nuclear Chemistry for Sustainable Fuel Cycles, "The EBR-II Legacy and Recent Advances" Procedia Chem. 7 (2012) 513–520.

[11] Pitner, A. L.; Baker, R. B. "Metal fuel test program" J. Nucl. Mater. 204 (1993) 124-130.

[12] Carmack, W. J. "Temperature and Burnup Correlated FCCI in U-10Zr Metallic Fuel" Ph.D. dissertation, University of Idaho (2012).

[13] Harp, J. M., personal communication, 2016.

[14] Okamoto, H. "Pd-Zr (Palladium-Zirconium)" J. Phase Equilib. 23(3) (2002) 290.

[15] Benson, M. T., et al., unpublished results.

[16] Mariani, R. D. et al., "Advanced Metallic Fuel for Ultra-High Burnup: Irradiation Tests in ATR" Transactions of the American Nuclear Society, NFSM 2012, Chicago, IL, June 2012.